J Mater Sci: Mater Electron (2016) 27:8682–8687
DOI 10.1007/s10854-016-4889-3

Facile approach to prepare TiO_2 nanofibers via electrospinning as anode materials for lithium ion batteries

Jing Li[1] · Hongdong Liu[1] · Zhongli Hu[1] · Yuan Chen[1] · Haibo Ruan[1] · Lei Zhang[2] · Rong Hu[1]

Received: 22 December 2015 / Accepted: 22 April 2016 / Published online: 27 April 2016

Abstract TiO_2 is considered to be a promising alternative anode material for lithium ion batteries. In this work, TiO_2 nanofibers have been successfully fabricated via electrospinning. The as-prepared products are characterized by X-ray diffraction, nitrogen adsorption–desorption and transmission electron microscopy. TiO_2 nanofibers are promising as anode materials for lithium ion batteries, which show good cycling performance and excellent rate capacity.

1 Introduction

Lithium ion batteries (LIBs) have been considered as new generation of green batteries for portable electronics and hybrid vehicles due to their high energy density, long cycle life and light weight [1–3]. Currently, carbon and graphite-based materials are widely used as the anodes for the traditional LIBs because of their natural abundance, low cost and excellent electrical conductivity [4]. However, commercial graphite with low theoretical capacity of 372 mAh g^{-1} that cannot meet the increasing demands for high capacity of LIBs [5, 6]. Therefore, it is a great urgent for us to find an ideal anode material with high energy density, excellent cyclic stability, and great rate capability [7, 8].

✉ Hongdong Liu
lhd0415@126.com

✉ Lei Zhang
leizhang0215@126.com

[1] Research Institute for New Materials Technology, Chongqing University of Arts and Sciences, Chongqing 402160, People's Republic of China

[2] College of Life Science, Chongqing Normal University, Chongqing 401331, People's Republic of China

Among the alternative materials, TiO_2 has been extensively studied due to its natural abundance, low cost, environmental friendliness, and superior safety [9, 10]. Moreover, the structural of TiO_2 is well stable during lithium insertion/extraction. Despite these advantages, TiO_2 suffers from low electronic conductivity, which will badly affect the electrochemical property and restrict the widespread application [11, 12]. What's more, the capacity retention of TiO_2 is limited due to the large irreversible capacity loss during the initial cycling [13]. One effective strategy to circumvent these limitations and improve the electrochemical performance is to fabricate nano-sized TiO_2 [14], such as nanospheres [15], nanofibers [16], nanosheets [17] and so on. Compared with the other morphologies, 1D nanofibers with large specific area can effectively shorten the diffusion distance of lithium ion, thus greatly improve the electrochemical property [18, 19]. Currently, in situ thermal oxidation [20], hydrothermal method [21] and electrospinning method [22] are the main methods for fabricating 1D nanostructure. Compared with the other methods, electrospinning can avoid to meet with the problem of low productivity and adding coagulants, thus to produce pure solid fibers from solution with diameters ranging from tens to hundreds of nanometers conveniently.

In this work, electrospinning was used to synthesis TiO_2 nanofibers. As anode materials for LiBs, we found that the reversible specific capacity of TiO_2 nanofibers remains a relatively high level after several cycles at high current density. The excellent results can be attributed to the unique nanofibers structure, which provides abundant channels for lithium ion transport, as well as accommodates volume variation. It demonstrates that TiO_2 nanofibers display high electrochemical performance.

2 Experimental

2.1 Synthesis of TiO_2 nanofibers

First of all, 32.83 mmol of N,N-Dimethylformamide (DMF) and 0.8 g of polyvinylpyrrolidone (PVP) were dissolved in 5.06 mL ethanol under continuous stirring. Then, 17.72 mmol of tetrabutyl titanate and 3 g of mineral oil were added into the above solution with mild mechanical stirring overnight. Next, the electrospinning progress was carried out under the condition of 18 kV applied voltage, and 1 ml/h solution fed rate. At last, the obtained precusors were calcined at 600 °C for 2 h in air at a heat rate of 5 °C min^{-1}, the TiO_2 nanofibers were prepared.

2.2 Materials characterization

The crystal structure analysis of the as-prepared samples was characterized using powder X-ray diffraction (XRD, TD-3500X) using Cu Ka radiation ($\lambda = 0.154056$ nm). The XRD pattern was recorded in the 2θ range of 10°–80° with a scan rate of 0.07°s^{-1}. The nitrogen adsorption–desorption isotherms and pore size distribution were measured at 77 K with a Quantachrome Autosorb-3B analyzer (USA). The surface morphology and microstructure of TiO_2 were characterized by transmission electron microscopy (TEM, JEM-2100).

2.3 Electrochemical characterization

2032-type coin cells were used to perform electrochemical measurements, which were assembled in an argon-filled glove box with the concentration of oxygen and water below 0.1 ppm. The working electrodes were prepared by mixing the active material, acetylene black and polyvinylidene fluoride (PVDF) in a weight ratio of 8:1:1 in N-methyl-2-pyrrolidone (NMP) to form homogeneous slurry. Next, the slurry uniformly coated onto Cu foil and dried at 120 °C for 12 h under vacuum condition. Pure lithium foil was used as the counter electrode and 1 M of $LiPF_6$ in ethylene carbonate (EC) and dimethyl carbonate (DMC) (1:1 v/v) as the electrolyte. The Galvanostatic charge/discharge tests were carried out on a Neware battery testing system in the potential range of 0–3.0 V at various current densities.

3 Results and discussions

The whole synthetic procedure of TiO_2 nanofibers is shown in Fig. 1, which is composed of the electrospinning and the calcinations process. The TiO_2 solution polymer is used to form a kind of fiberillous precursor through electrospinning progress with a high voltage, which provides a great electric field force to change the forms of the TiO_2 polymer from solution into jet trickle. The trickle can evaporate or solidify during the process of the spray, thus the TiO_2 solution lands on the collector to form a continuous fiberillous TiO_2 precursor. It apparently shows that the nanofibers are composed of many uniformly distributed small PVP and TiO_2 grains before calcinations. Lastly, the small PVP grains can disappear and leave the TiO_2 alone here to form a special nanofiber structure after the calcinations.

To verity the morphology of the TiO_2 sample by electrospinning, the transmission electron microscopy (TEM) was performed. Figure 2a shows a typical transmission electron microscopy (TEM) image of TiO_2 nanofibers. It can be clearly observed that the as-synthesized TiO_2 displays a line-like morphology with a length from several micrometers to a few tens of micrometers. As shown in a typical high magnification TEM image in Fig. 2b, the TiO_2 is composed of well-defined nanofibers with average diameter of 176 nm approximately. In addition, as seen from Fig. 2b, TiO_2 nanofibers with many mesopores,

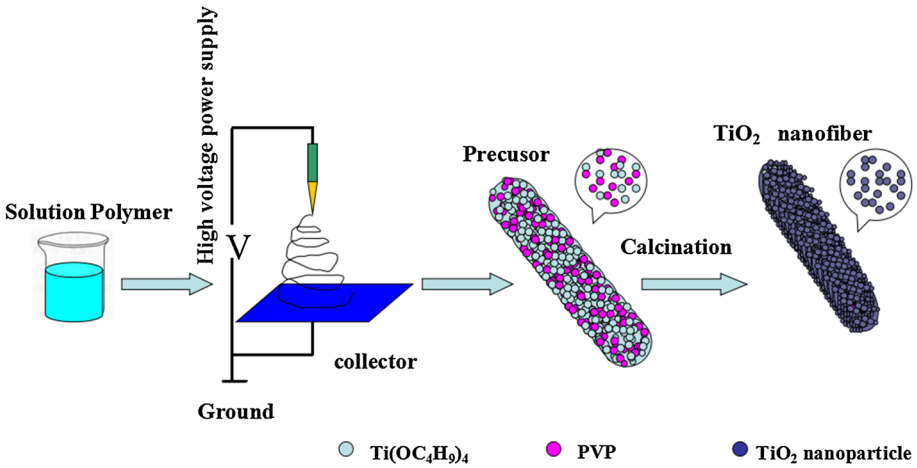

Fig. 1 Process of the preparation of TiO_2 nanofibers

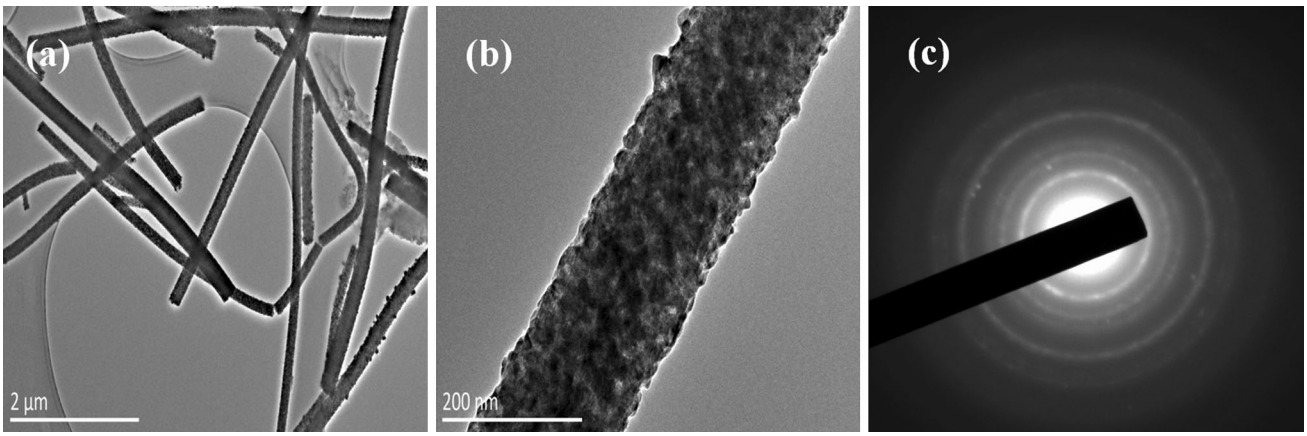

Fig. 2 **a**, **b** TEM images with different magnifications of TiO_2 nanofibers and **c** SAED pattern of TiO_2 nanofibers

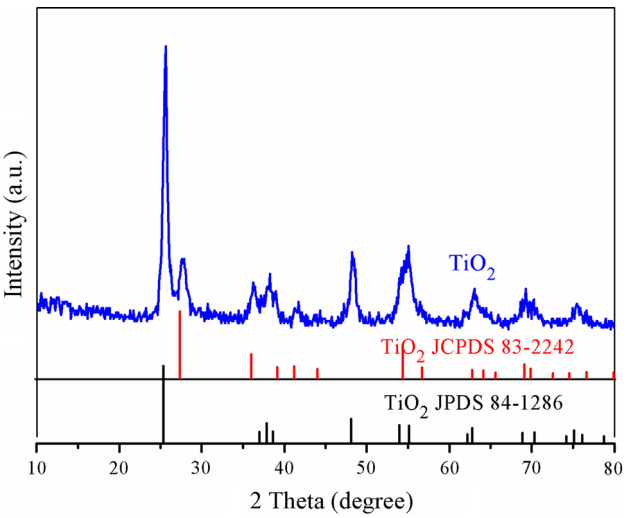

Fig. 3 XRD pattern of TiO_2 nanofibers

which can provide abundant channels for lithium ion transport, shorten the lithium diffusion length and possess high electrochemical activity. The crystallinity of the nanofibers is clearly supported from the selected area electron diffraction pattern (SAED) in Fig. 2c, which shows well-defined concentric rings. It obviously represents that there are no appreciable changes in the morphological features, confirming the formation of the TiO_2 crystal.

As observed in Fig. 3, the diffraction peaks of 2θ values located at 25.3, 37.9, 48.1, 54.0, 55.1 and 62.8° can be indexed to (101), (004), (200), (105), (211) and (204) planes of the anatase structure of TiO_2 (JCPDS 84-1286). The other peaks at 27.4 and 55.4° correspond to the (110), and (211) crystal faces of rutile TiO_2 (JCPDS 83-2242), respectively.

Figure 4 shows the nitrogen adsorption–desorption isotherm and pore size distribution curve. As seen in Fig. 4a,

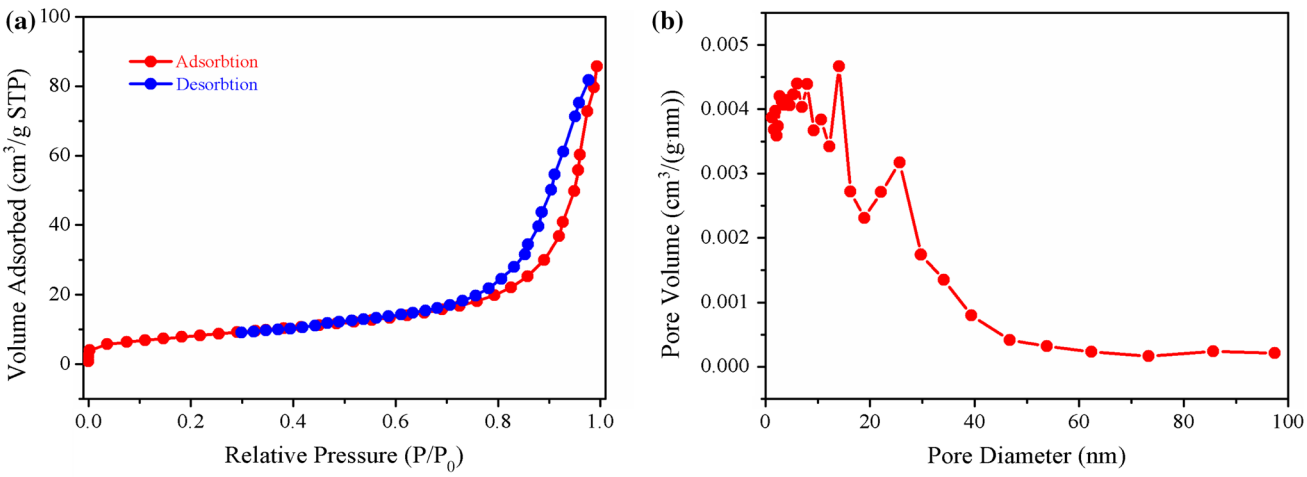

Fig. 4 **a** Nitrogen adsorption–desorption isotherm, **b** Pore size distribution curve

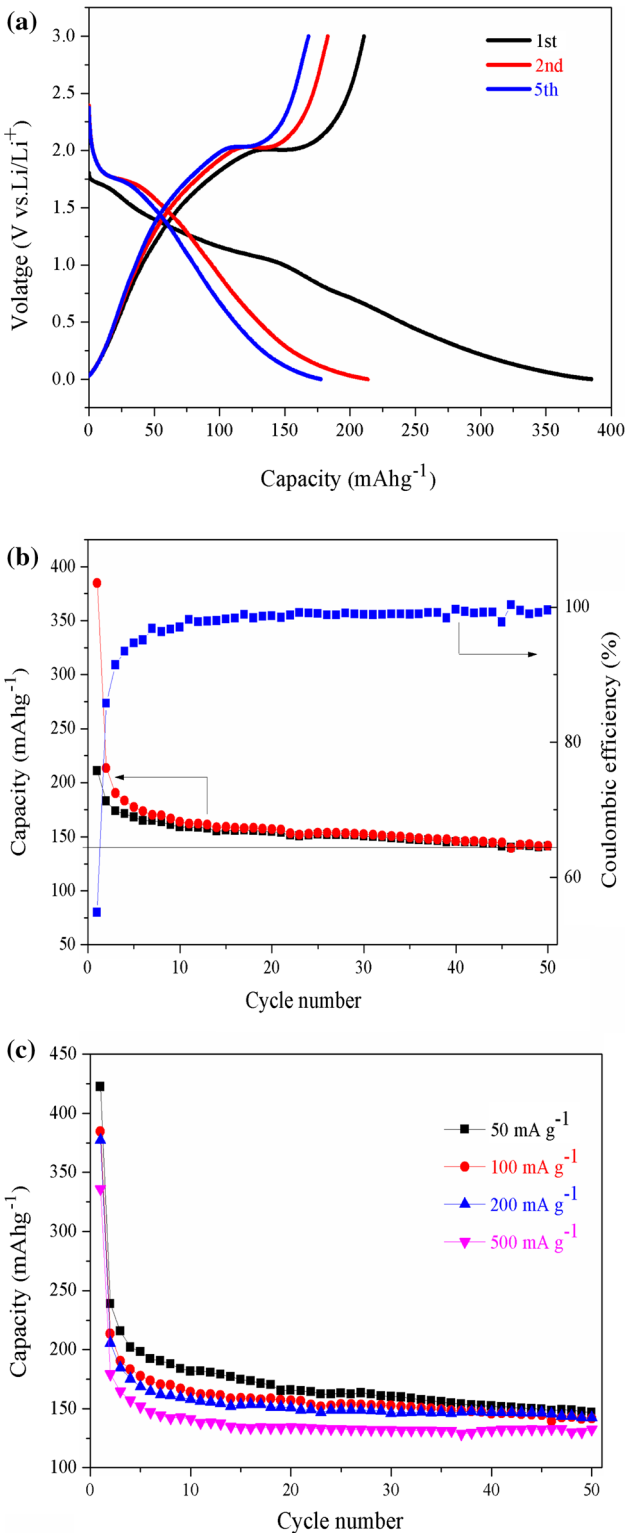

Fig. 5 **a** Charge–discharge profiles of TiO_2 nanofibers electrodes at 100 mA g^{-1}, **b** Cycling performance and coulombic efficiency of TiO_2 nanofibers between 0 and 3.0 V versus Li/Li^+ at the current density of 100 mA g^{-1}, **c** Rate performance of TiO_2 nanofibers electrodes at the current density from 50 to 500 mA g^{-1}

the samples exihibit a typical type IV nitrogen adsorption–desorption isotherm with a H3 hysteresis loop according to the IUPAC classification, which indicates that the presence of mesopores in TiO_2 nanofibers. The Brunauer–Emmett–Teller (BET) specific surface area caluated from the isotherm is 28.3 m^2 g^{-1}. From the Barrette Joynere Halenda (BJH) analysis in Fig. 4b, it is can be observed that the samples have a broad pore size distribution and a mean pore size is 18.05 nm. Such porous structure with suitable specific surface area can provide lots of electrochemical activity sites for Li^+ and short the elecrton and Li^+ diffusion pathway during lithiation/delithiation process, which result in the TiO_2 samples with an excellent electrochemical performance.

The electrochemical performance of TiO_2 nanofibers which were evaluated by galvanostatic charge/discharge measurement at the current density of 100 mA g^{-1} in a voltage of 0–3.0 V. The 1st, 2nd and 5th discharge–charge curves are shown in Fig. 5a. The first discharge and charge capacities are 385 and 211 mAh g^{-1}, respectively, with initial coulomb efficiency of 54.8 %. The initial irreversible capacity lossing can be ascribed to the solid electrolyte interface (SEI) layer which is formed on the surface of the electrode material by the decomposition of the electrolyte during the first discharge process and incomplete conversion reaction as expressed in the following Eq. (1) [23, 24]. During the 2nd cycle, the discharge capacity decreases to 213 mAh g^{-1} with a corresponding charge capacity of 183 mAh g^{-1}, and the coulomb efficiency increases rapidly to 85.9 %. It is worth noticing that the value of coulombic efficiency further improves to 94.4 % in the 5th cycle. The profiles with discharge and charge plateaus located at 1.75 and 2.0 V in the first cycle, respectively, which suggest that the Li^+ insertion and extraction within the TiO_2 samples. However, the voltage plateaus have no appreciable changes during the following discharge and charge process, indicating that the TiO_2 nanofibers exist an excellent cycling stability.

$$TiO_2 + xLi^+ + xe^- \rightarrow Li_xTiO_2 \quad (1)$$

To further highlight the cycling performance of TiO_2 nanofibers, charge–discharge for 50 cycles at the current rate of 100 mAg^{-1} between 0 and 3.0 V was measured, and as presented in Fig. 5b. The TiO_2 electrode exhibits an initial discharge capacity of 384.7 mAh g^{-1} with an irreversible capacity of 174 mAh g^{-1}. The initial irreversible capacity loss of TiO_2 electrode can be ascribed to the electrolyte decomposition and the formation of SEI film, which is common in metal oxide anodes [25, 26]. The discharge capacity dramatically and rapidly drops to 186 mAh g^{-1} after the first three cycles. From the fourth

cycle, the specific capacity slowly decreases and retains 141.7 mAh g^{-1} over 50 cycles. In addition, TiO_2 nanofibers process a high coulombic efficiency of 99 % during the subsequent cycles except the previous three cycles. These results imply that the Li intercalation and de-intercalation reaction become more reversible with the increase of the cycle number.

Figure 5c shows the reversible capacities of TiO_2 nanofibers at various current densities from 0 to 3.0 V. In the first cycle, TiO_2 nanofibers display a discharge capacity of 422.4 mAh g^{-1} at the current densities of 50 mA g^{-1}, 384.7 mAh g^{-1} at 100 mA g^{-1}, 377.2 mAh g^{-1} at 200 mA g^{-1}, and 335.9 mAh g^{-1} at 500 mA g^{-1}. After several cycles, the discharge capacities of TiO_2 samples at various current densities become more stability. It can be clearly observed that the electrode still maintains a discharge capacity of 146.7 mAh g^{-1} over 50 cycles at the current densities of 50 mA g^{-1}, when the current density is increased to 100 and 200 mA g^{-1}, the discharge capacity slightly reduces to 142.4 and 141.7 mAh g^{-1}, respectively. Even at the current density of 500 mAh g^{-1}, it can still retain a discharge capacity of 132.4 mAh g^{-1} after 50 cycles. Obviously, TiO_2 nanofibers exhibit excellent rate performance.

4 Conclusions

In summary, we report a facile and simple method for synthesis TiO_2 nanofibers via electrospinning. The as-synthesized TiO_2 shows a line-like porous structure which providing abundant channels for lithium ion transport and shorten the lithium diffusion length. When used as anode materials for LIBs, it exhibits excellent cycling stability and good rate performance. It depicts a specific capacity of 142.4 mAh g^{-1} at a discharge rate of 100 mA g^{-1} after 50 cycles, even the current density is increased to 500 mA g^{-1}, it also displays a high specific capacity of 132.4 mAh g^{-1}. All these results indicate that TiO_2 nanofibers are good candidates as high-performance anode materials for LIBs.

Acknowledgments This work was financially supported by Basic and Frontier Research Program of Chongqing Municipality (cstc2015jcyjA90020) and (cstc2014jcyjA10063), Scientific and Technological Research Program of Chongqing Municipal Education Commission (KJ1501101), (KJ1500323) and (KJ1501116), Introduction of Talent Project of Chongqing University of Arts and Sciences (R2013CJ06), China Postdoctoral Science Foundation (2015M582499), Postdoctoral special Foundation of Chongqing (Xm2015064) and Project of Chongqing Normal University (14XYY025) and (14XLB004), and National Natural Science Foundation of China (51502030).

References

1. W. Wei, S. Yang, H. Zhou, I. Lieberwirth, X. Feng, K. Muellen, 3D graphene foams cross-linked with pre-encapsulated Fe_3O_4 nanospheres for enhanced lithium storage. Adv. Mater. **25**, 2909–2914 (2013)
2. Z. Zeng, H. Zhao, P. Lv, Z. Zhang, J. Wang, Q. Xia, Electrochemical properties of iron oxides/carbon nanotubes as anode material for lithium ion batteries. J. Power Sources **274**, 1091–1099 (2015)
3. X. Dong, L. Li, C. Zhao, H.K. Liu, Z. Guo, Controllable synthesis of RGO/Fe_xO_y nanocomposites as high-performance anode materials for lithium ion batteries. J. Mater. Chem. A **2**, 9844–9850 (2014)
4. Z.X. Huang, Y. Wang, Y.G. Zhu, Y. Shi, J.I. Wong, H.Y. Yang, 3D graphene supported MoO_2 for high performance binder-free lithium ion battery. Nanoscale **6**, 9839–9845 (2014)
5. J. Wang, L. Shen, H. Li, X. Wang, P. Nie, B. Ding, G. Xu, H. Dou, X. Zhang, A facile one-pot synthesis of TiO_2/nitrogen-doped reduced graphene oxide nanocomposite as anode materials for high-rate lithium-ion batteries. Electrochim. Acta **133**, 209–216 (2014)
6. P. Wang, M. Gao, H. Pan, J. Zhang, C. Liang, J. Wang, P. Zhou, Y. Liu, A facile synthesis of Fe_3O_4/C composite with high cycle stability as anode material for lithium-ion batteries. J. Power Sources **239**, 466–474 (2013)
7. P. Lv, H. Zhao, Z. Zeng, J. Wang, T. Zhang, X. Li, Facile preparation and electrochemical properties of carbon coated Fe_3O_4 as anode material for lithium-ion batteries. J. Power Sources **259**, 92–97 (2014)
8. C. Mao, F. Du, G. Li, Facile synthesis of hierarchically porous hematite nanostructures composed of aligned nanorods for superior lithium storage capability. J. Power Sources **272**, 997–1002 (2014)
9. J. Sundaramurthy, V. Aravindan, P.S. Kumar, S. Madhavi, S. Ramakrishna, Electrospun TiO_2-delta nanofibers as insertion anode for Li-Ion battery applications. J. Phys. Chem. C **118**, 16776–16781 (2014)
10. X. Li, Y. Zhang, T. Li, Q. Zhong, H. Li, J. Huang, Graphene nanoscrolls encapsulated TiO_2 (B) nanowires for lithium storage. J. Power Sources **268**, 372–378 (2014)
11. E. Liu, J. Wang, C. Shi, N. Zhao, C. He, J. Li, J.-Z. Pang, Anomalous interfacial lithium storage in graphene/TiO_2 for lithium ion batteries. ACS Appl. Mater. Interfaces **6**, 18147–18151 (2014)
12. J. Jin, S.Z. Huang, J. Liu, Y. Li, D.-S. Chen, H.-E. Wang, Y. Yu, L.-H. Chen, B.-L. Su, Design of new anode materials based on hierarchical, three dimensional ordered macro mesoporous TiO_2 for high performance lithium ion batteries. J. Mater. Chem. A **2**, 9699–9708 (2014)
13. S.M. Oh, J.Y. Hwang, C.S. Yoon, J. Lu, K. Amine, I. Belharouak, Y.-K. Sun, High electrochemical performances of microsphere C-TiO2 anode for sodium-ion battery. ACS Appl. Mater. Interfaces **6**, 11295–11301 (2014)
14. Z.J. Zhang, Q.-Y. Zeng, S.-L. Chou, X.-J. Li, H.-J. Li, K. Ozawa, H.-K. Liu, J.-Z. Wang, Tuning three-dimensional TiO_2 nanotube electrode to achieve high utilization of Ti substrate for lithium storage. Electrochim. Acta **133**, 570–577 (2014)
15. X. Wang, Y. Wang, L. Yang, K. Wang, X. Lou, B. Cai, Template-free synthesis of homogeneous yolkeshell TiO_2 hierarchical microspheres for high performance lithium ion batteries. J. Power Sources **262**, 72–78 (2014)
16. Z. Jin, M. Yang, G. Wang, J. Wang, Y. Luan, L. Tan, Y. Lu, Hierarchical architectures of TiO_2 nanowires-CNT

interpenetrating networks as high-rate anodes for lithium-ion batteries. Nanotechnology **25**, 395–401 (2014)
17. F. Wu, Z. Wang, X. Li, H. Guo, Simple preparation of petal-like TiO_2 nanosheets as anode materials for lithium-ion batteries. Ceram. Int. **40**, 16805–16810 (2014)
18. D.A. Zhang, Q. Wang, Q. Wang, J. Sun, L.-L. Xing, X.-Y. Xue, Core–shell SnO_2@TiO_2–B nanowires as the anode of lithium ion battery with high capacity and rate capability. Mater. Lett. **128**, 295–298 (2014)
19. Q. Tian, Z. Zhang, L. Yang, S.-I. Hirano, Encapsulation of SnO_2 nanoparticles into hollow TiO2 nanowires as high performance anode materials for lithium ion batteries. J. Power Sources **253**, 9–16 (2014)
20. A. Li, H. Song, W. Wan, J. Zhou, X. Chen, Copper oxide nanowire arrays synthesized by in situ thermal oxidation as an anode material for lithium-ion batteries. Electrochim. Acta **132**, 42–48 (2014)
21. D. Su, H.-J. Ahn, G. Wang, One-dimensional magnetite Fe_3O_4 nanowires as electrode material for Li-ion batteries with improved electrochemical performance. J. Power Sources **244**, 742–746 (2013)
22. D. Baiyila, X. Wang, X. Li, B. Sharileaodu, X. Li, L. Xu, Z. Liu, L. Duan, J. Liu, Electrospun TiO_2 nanofibers integrating space-separated magnetic nanoparticles and heterostructures for recoverable and efficient photocatalyst. J. Mater. Chem. A **2**, 12304–12310 (2014)
23. Z. Yan, L. Liu, H. Guo, J. Tan, H. Shu, X. Yang, H. Hu, Q. Zhou, Z. Huang, X. Wang, One-pot synthesis of FCNTs-wired TiO_2 nanocomposites as anode materials for high-rate lithium ion batteries. Electrochim. Acta **123**, 551–559 (2014)
24. X. Wang, Y. Wang, L. Yang, K. Wang, X. Lou, B. Cai, Template-free synthesis of homogeneous yolkeshell TiO_2 hierarchical microspheres for high performance lithium ion batteries. J. Power Sources **262**, 72–78 (2014)
25. L. Fan, B. Li, D.W. Rooney, N. Zhang, K. Sun, In situ preparation of 3D graphene aerogels@hierarchical Fe_3O_4 nanoclusters as high rate and long cycle anode materials for lithium ion batteries. Chem. Commun. **51**, 1597–1600 (2015)
26. H.B. Lin, H.B. Rong, W.Z. Huang, Y.H. Liao, L.D. Xing, M.Q. Xu, X.P. Li, W.S. Li, Triple-shelled Mn_2O_3 hollow nanocubes: force induced synthesis and excellent performance as the anode in lithium-ion batteries. J. Mater. Chem. A **2**, 14189–14194 (2014)